Hindawi
International Journal of Aerospace Engineering
Volume 2021, Article ID 9051131, 11 pages
https://doi.org/10.1155/2021/9051131

Research Article

FDA-MIMO Beampattern Synthesis with an Analytical Method

Changlin Zhou,[1] **Chunyang Wang**,[1] **Jian Gong**,[1] **Ming Tan**,[2] **Yingjian Zhao**,[1] **and Mingjie Liu**[1]

[1]*Air and Missile Defense College, Air Force Engineering University, Xi'an, Shanxi 710051, China*
[2]*College of Information and Communication, National University of Defense Technology, Wuhan, Hubei 430000, China*

Correspondence should be addressed to Chunyang Wang; wangcy_kgd@163.com

Received 26 August 2021; Accepted 22 October 2021; Published 13 November 2021

Academic Editor: Linda L. Vahala

Since the beampattern has the characteristics of range-angle dependence, frequency diverse array multiple-input multiple-output (FDA-MIMO) radar has a good application prospect. There have been many studies to improve the performance of the beampattern by optimizing the frequency offset. However, on the basis of fully understanding the time parameters, the relationship between the array element frequency offset and the beampattern performance still needs to be clarified. Based on a new FDA-MIMO radar framework, this paper presents an analytical solution of the beampattern, which removes the influence of the time parameter. Taking the minimum main lobe as the objective function, an analytical method for solving a better frequency offset is given. Then, a method of using the window function was proposed to reduce the high side lobes of the range dimension. Comparing with the existing FDA radar beampattern design methods, it can achieve a more focusing beampattern. The simulation results verify the correctness of the theory.

1. Introduction

Since FDA has been first proposed in [1], it has received extensive attention and research from scholars at home and abroad, because its beampattern is range-angle-depend and time-variant [2, 3]. FDA radar has great application value because of its ability of range-angle-dependent [4–6]. To improve its application value, the literature [7–11] studied the time-variant problem of FDA radar. The literature [11] considers the FDA-MIMO radar scheme proposed in [12, 13], which form time-invariant beampattern.

The study of FDA beampattern is a vital issue. A logarithmic increase frequency offset scheme was proposed in [14], which can form spot beams in space. The design of frequency offset using window function is another important research direction [15–17]. These methods are all numerical solutions based on the comparison of effects, but there are countless possibilities for numerical solutions. And they did not consider the influence of time parameters. Considering the influence of time parameters [11], a method of increasing frequency combined with window function is proposed in [18]. It is still a numerical solution. In addition to numerical solutions, many scholars have explored the use of heuristic algorithms to obtain the optimal frequency offset [19–21]. However, when the target position changes, the frequency offset needs to be optimized again, which consumes a lot of computing resources. The problem is particularly prominent in large arrays. The most ideal solution is to obtain an analytical solution of the frequency offset, which was discussed in [22] using FDA radar. However, [22] did not consider the influence of time parameters, and the obtained beampattern is an instantaneous beampattern, which cannot be used to track targets.

Therefore, it is vital to get rid of the disadvantages of the FDA beampattern such as range-angle coupling and time-variant. In this paper, we use the FDA-MIMO radar system to obtain the analytical solution of the beampattern. And the beampattern is range-dependent and time-invariant. The main contributions of this paper are as follows:

(1) Through phase modulation, the FDA-MIMO radar system we designed can form a spot beam at any

position in space. Literature [11] activates the range-dependent property of FDA through the signal processing at the receiver, and the matched filtering at the receiver is related to the frequency offset of the transmitting array element. Opposed to it, this paper weights the transmitted signal so that all the parameters related to the frequency offset are designed at the transmitter. The modulation phase of each element is a function of frequency offset and target position. Moreover, the frequency offset is only related to the number of transmitting array elements

(2) In FDA-MIMO radar, the mathematical relationship between frequency offset and range-angle beampattern has not been clarified, such as [18]. Through the simplified approximation of the pattern, we get that the spot beam formed by the FDA-MIMO radar is a quadratic curve related to the frequency offset, which mathematically explains how the frequency offset affects the performance of the beampattern

(3) We minimize the main lobe area of the FDA-MIMO radar beampattern to obtain the optimal frequency offset that is only related to the number of array elements. Therefore, the frequency offset is optimal for the target at any position in the space. Finally, the side lobes of the range dimension are reduced by using a Kaiser window function

The rest of the paper is organized as follows. In Section 2, we rederived the beamforming theory of the FDA-MIMO radar. Then, a method is proposed to activate the range dependence of FDA-MIMO radar. In Section 3, through a series of approximate simplified calculations, we derive the analytical expression of the FDA-MIMO radar beampattern that depends on the frequency offset. By setting all frequency offsets to 0, the phased array radar beampattern expression is obtained, which further verifies the feasibility of this method. In Section 4, by minimizing the main lobe area of the beampattern, we derive a better offset to form the spot beampattern of the FDA-MIMO radar. In Section 5, we provide some simulations. Finally, concluding summaries are drawn in Section 6.

Notation. We use boldface for vectors $\boldsymbol{a}$ and matrices $\boldsymbol{A}$. Scalar a is denoted by italicized. The transpose and the conjugate are denoted by the symbols $(\bullet)^T$ and $(\bullet)^*$, respectively. $\boldsymbol{I}_M$ and $\boldsymbol{E}_M$ denote $M \times M$-dimensional identity matrix and all-one matrix, respectively. The letter j represents the imaginary unit (i.e., $j = \sqrt{-1}$).

2. Analysis of FDA-MIMO Radar System

We consider a collocated narrowband FDA-MIMO radar system with M transmitting antennas and N receiving antennas. Both the transmitting array and the receiving array are uniform linear arrays. The distance between transmitting array elements is d_T, and the distance between receiving array elements is d_R. The carrier frequency of the transmitted signal is f_0. Its configuration is shown in Figure 1.

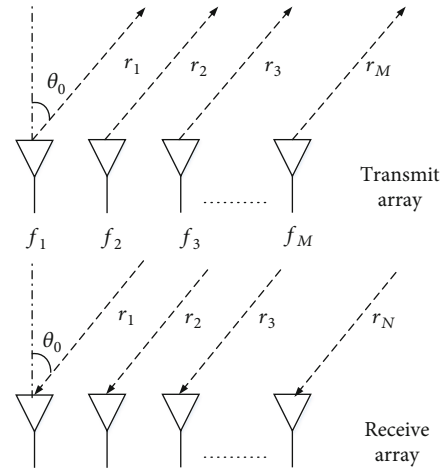

Figure 1: The conventional configuration of FDA-MIMO.

The frequency offset of the m-th element is $f(m)$; then, the transmitting frequency is

$$f_m = f_0 + f(m), \quad m = 1, 2, \cdots, M. \tag{1}$$

Consider [11], the transmitted signal at time t of the m -th element is

$$s_m(t) = \psi_m(t) e^{j2\pi f_m t}, \tag{2}$$

where $\psi_m(t)$ is the baseband envelope of the m-th transmitting array element, which satisfies orthogonality:

$$\int {\psi_{m1}}^*(t) \cdot \psi_{m2}(t-\tau) dt = 0, \quad \mathrm{m1} \neq m2, \forall \tau. \tag{3}$$

We add phase modulation to each transmitting array element, which is easy to implement for MIMO radar. Therefore, equation (2) can be rewritten as:

$$s_m(t) = \psi_m(t) e^{j\Phi_m(t)} e^{j2\pi f_m t}. \tag{4}$$

Observed from the desired target at (r, θ). The received signal related to the m-th transmitting element and the n -th receiving element can be expressed as:

$$s_{m,n}(t-\tau_{m,n}) = \psi_n(t-\tau_{m,n}) e^{j\Phi_m(t--\tau_{m,n})} \cdot e^{j2\pi(f_0+f(m))(t-\tau_{m,n})}, \quad n = 1, 2 \cdots, N, \tag{5}$$

where $\tau_{m,n} = 2r/c - md_T \sin\theta/c - nd_R \sin\theta/c$ represents the transmit delay.

In the case of far-field narrowband, (5) can be approximately expressed as [11]:

$$s_{m,n}\left(t'\right) = \psi_m\left(\frac{t}{2r/c}\right) e^{j\Phi_m(t')} e^{j\varphi_n(t')} = \psi_m\left(t'\right) e^{j\Phi_m(t')} e^{j\varphi_n(t')}, \tag{6}$$

where t' is the time index within pulse and $\varphi_n(t')$ can be expressed as:

$$\begin{aligned}\varphi_n\left(t'\right) &= 2\pi\int_0^{t'+((md_T\ \sin\theta/c)+(nd_R\ \sin\theta/c))}(f_0+f(m))\,dx \\ &= 2\pi\left(f_0t'+f(m)t'+f_0\frac{md_T\sin\theta}{c}+f_0\frac{nd_R\sin\theta}{c}\right. \\ &\quad \left.+f(m)\frac{md_T\sin\theta}{c}+f(m)\frac{nd_R\sin\theta}{c}\right).\end{aligned} \tag{7}$$

Because $f(m) \ll f_0$, (7) can be reapproximated as:

$$\begin{aligned}\varphi_n\left(t'\right) &= 2\pi\int_0^{t'+((md_T\ \sin\theta/c)+(nd_R\ \sin\theta/c))}(f_0+f(m))\,dx \\ &= 2\pi\left(f_0t'+f(m)t'+f_0\frac{md_T\sin\theta}{c}+f_0\frac{nd_R\sin\theta}{c}\right).\end{aligned} \tag{8}$$

Bring (8) into (6) and note that $t = t' + 2r/c$, (6) can be rewritten as:

$$\begin{aligned}&s_{m,n}\left(t'\right) = \psi_m\left(t'\right)e^{j\Phi_m\left(t'\right)}, \\ &e^{j2\pi\left(f_0t'+f(m)t'+f_0(md_T\ \sin\theta/c)+f_0(nd_R\ \sin\theta/c)\right)} = \psi_m\left(t'\right)e^{j\Phi_m\left(t'\right)}, \\ &e^{j2\pi(f_0t-f_0(2r/c)+f(m)t-f(m)(2r/c)+f_0(md_T\ \sin\theta/c)+f_0(nd_R\ \sin\theta/c))}.\end{aligned} \tag{9}$$

The received signal is first mixed with $e^{-j2\pi f_0 t}$ in the analog signal processor and then mixed with $\psi_m(t')$ in the digital signal processor, as shown in Figure 2.

Then, the relative output of the m-th transmitting array element and the n-th receiving array element can be expressed as:

$$\begin{aligned}&s_{m,n}^{\text{Output}}\left(t'\right) = \xi_s e^{j\Phi_m\left(t'\right)}, \\ &e^{j2\pi(-f_0(2r/c)+f(m)t-f(m)(2r/c)+f_0(md_T\ \sin\theta/c)+f_0(nd_R\ \sin\theta/c))}.\end{aligned} \tag{10}$$

ξ_s is the signal complex coefficient after matched filtering. The array factor can be expressed as:

$$\begin{aligned}AF = \sum_{m=1}^{M}\sum_{n=1}^{N}s_{m,n}^{\text{Output}}\left(t'\right) &= \xi_s e^{-j2\pi f_0(2r/c)} \\ &\cdot\sum_{m=1}^{M}\sum_{n=1}^{N}\frac{e^{j\Phi_m\left(t'\right)}e^{j2\pi f(m)t}}{e^{j2\pi(-f(m)(2r/c)+f_0(md_T\ \sin\theta/c)+f_0(nd_R\ \sin\theta/c))}}.\end{aligned} \tag{11}$$

In order to detect the target at (r_t, θ_t), the phase modulation of the m-th transmitting array element is given as:

$$\begin{aligned}\Phi_m\left(t'\right) &= -2\pi f(m)t + 2\pi f(m)\frac{2r_t}{c} - 2\pi f_0\frac{md_T\sin\theta_t}{c} \\ &\quad - 2\pi f_0\frac{nd_R\sin\theta_t}{c}.\end{aligned} \tag{12}$$

Bring (12) into (11), then (11) can be rewritten as:

$$\begin{aligned}AF = \xi_s e^{-j2\pi f_0(2r/c)}&\sum_{m=1}^{M}e^{j(4\pi/c)f(m)(r_t-r)}e^{j(2\pi f_0 md_T(\sin\theta-\sin\theta_t)/c)} \\ &\cdot\sum_{n=1}^{N}e^{j(2\pi f_0 nd_R(\sin\theta-\sin\theta_t)/c)}.\end{aligned} \tag{13}$$

Therefore, the transmit-receive normalized beampattern is expressed as:

$$\begin{aligned}B = &\left|\sum_{m=1}^{M}e^{j(4\pi/c)f(m)(r_t-r)}e^{j(2\pi f_0 md_T(\sin\theta-\sin\theta_t)/c)}\right|^2 \\ &\cdot\left|\sum_{n=1}^{N}e^{j(2\pi f_0 nd_R(\sin\theta-\sin\theta_t)/c)}\right|^2.\end{aligned} \tag{14}$$

The transmitting-receiving beampattern can be further equivalent to the transmitting beampattern and the receiving beampattern at the receiving end, and the transmitting beampattern can be expressed as:

$$B_T = \left|\sum_{m=1}^{M}e^{j(4\pi/c)f(m)(r_t-r)}e^{j(2\pi f_0 md_T(\sin\theta-\sin\theta_t)/c)}\right|^2. \tag{15}$$

The receiving beampattern can be expressed as:

$$B_R = \left|\sum_{n=1}^{N}e^{j(2\pi f_0 nd_R(\sin\theta-\sin\theta_t)/c)}\right|^2. \tag{16}$$

(14) indicates that the FDA-MIMO radar produces a range-dependent beam with time-invariant characteristics. And regardless of the value of the frequency offset, the FDA-MIMO radar beampattern can achieve the maximum M^2N^2 at the target point. (15) and (16) indicate that the equivalent receiving beampattern only affects the angle characteristics, while the equivalent transmitting beampattern can affect the angle and range characteristics. Therefore, when designing the FDA-MIMO radar, the variables related to the frequency offset should be implemented at the transmitter. The configuration is shown in Figure 3.

$\Phi_m(t')$ is the variable about frequency offset and target space position. Therefore, we can activate the range dependence of FDA-MIMO radar by setting $\Phi_m(t')$.

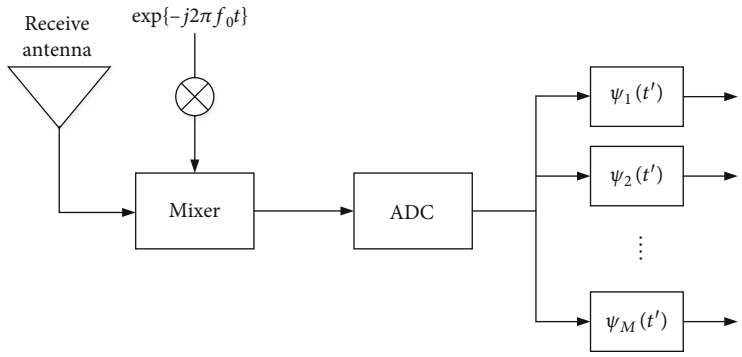

Figure 2: The signal processing at receiver.

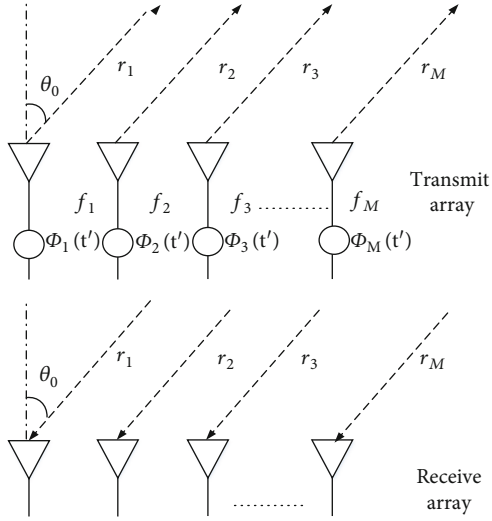

Figure 3: Our proposed configuration of FDA-MIMO.

3. Analytical Expression of the FDA-MIMO Radar Beampattern

We hope to form a spot beampattern that can only rely on (15), because (16) shows that the equivalent receiving beampattern can only affect the angular resolution. We use half-power beamwidth to analyze the FDA-MIMO radar equivalent transmitting beampattern. The FDA-MIMO radar equivalent transmitting beampattern can achieve the maximum M^2 at the target point. (r_h, θ_h) are those points where the power decays by half.

$$\begin{aligned} B_T &= \left| \sum_{m=1}^{M} e^{j(4\pi/c)f(m)(r_t - r_h)} e^{j(2\pi f_0 m d_T(\sin\theta_h - \sin\theta_t)/c)} \right|^2 \\ &= \left| \sum_{m=1}^{M} e^{jy_m} \right|^2 = \frac{M^2}{2}, \end{aligned} \tag{17}$$

where $y_m = Af(m) + Bm$, $A = -(4\pi/c)(r_h - r_t)$, $B = (2\pi f_0 d_T/c)(\sin\theta_h - \sin\theta_t)$. By Euler's formula and Taylor approximation, it can be expressed as [22]:

$$\begin{aligned} \left| \sum_{m=1}^{M} e^{jy_m} \right|^2 &= \left(\sum_{m=1}^{M} \cos(y_m) \right)^2 + \left(\sum_{i=1}^{M} \cos(y_i) \right)^2 \\ &= \sum_{m=1}^{M} \sum_{i=1}^{M} \cos(y_m - y_i) \\ &\approx \sum_{m=1}^{M} \sum_{i=1}^{M} \left(1 - \frac{1}{2}(y_m - y_i)^2 \right) \\ &= \frac{M^2}{2}. \end{aligned} \tag{18}$$

Simplifying further, we can get:

$$\sum_{m=1}^{M} \sum_{i=1}^{M} (y_m - y_i)^2 = M^2. \tag{19}$$

Bring y_m into (19), and expand (19) to:

$$\sum_{m=1}^{M} \sum_{i=1}^{M} (y_m - y_i)^2 = A^2 a(f) + 2AB b(f) + B^2 \mathrm{g}(f) = M^2, \tag{20}$$

$$a(f) = \sum_{m=1}^{M} \sum_{i=1}^{M} (f(m) - f(i))^2, \tag{21}$$

$$b(f) = \sum_{m=1}^{M} \sum_{i=1}^{M} (f(m) - f(i))(m - i), \tag{22}$$

$$\mathrm{g}(f) = \sum_{m=1}^{M} \sum_{i=1}^{M} (m - i)^2 = \frac{M^2(M^2 - 1)}{6} = G. \tag{23}$$

When θ_h and θ_t are close, we introduce an approximation:

$$\sin\theta_h - \sin\theta_t \approx (\theta_h - \theta_t)\cos(\theta_t). \tag{24}$$

This is true when forming a spot beam. Bringing (24) into (20), we can further get:

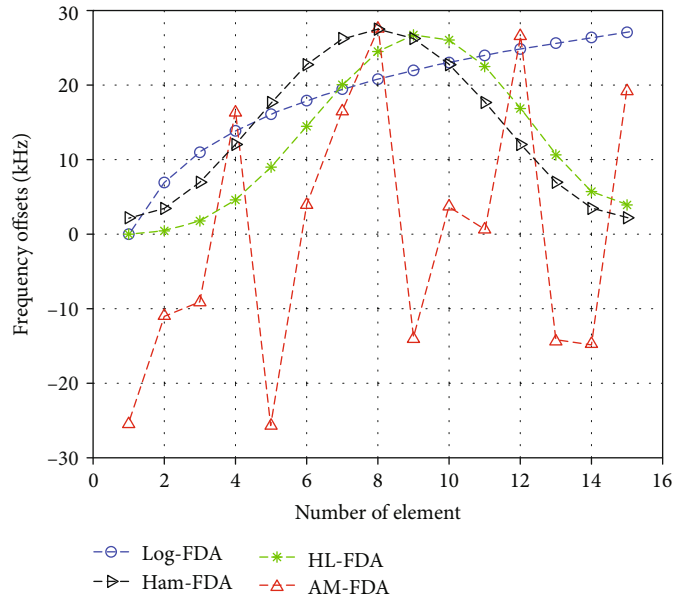

Figure 4: Frequency offset comparison.

$$M^2 = a(f)\left(\frac{4\pi}{c}\right)^2 (r_h - r_t)^2 - b(f)\left(\frac{4\pi}{c}\right)^2 f_0 d_T \cos(\theta_t)(\theta_h - \theta_t) + G\left(\frac{2\pi f_0 d_T \cos\theta_t}{c}\right)^2 (\theta_h - \theta_t)^2. \tag{25}$$

(25) represents the analytical expression of the equivalent transmit beampattern produced by the frequency offset **f**. It is a quadratic curve with (r_h, θ_h) as the boundary and the target point (r_t, θ_t) as the center in the angle-range plane. Using the Cauchy-Schwarz inequality, it is easy to prove $\Delta = a(f)G - b(f)^2 \geq 0$. Therefore, its beampattern can only be ellipses ($\Delta > 0$) and parallel lines ($\Delta = 0$).

When all frequency offsets are set to zero, it is equivalent to phased array radar. At this time $a(f) = 0$, $b(f) = 0$, and $\Delta = 0$.

At this time, (25) can be expressed as:

$$(\theta_h - \theta_t)^2 = \frac{6}{(M^2 - 1)(2\pi f_0 d_T \cos\theta_t / c)^2}. \tag{26}$$

Obviously, the pattern has no range dependence, and its main lobe is a set of parallel lines centered on θ_t and bounded by θ_h. The results are consistent with the phased array radar, further verifying the correctness of the derivation.

4. Optimal Frequency Offset Design

It is a vital problem we must solve that how to evaluate the impact of different frequency offset on the performance of the main lobe when optimizing the frequency offset. Because it is an ellipse on the range-angle plane, we naturally think of minimizing the area of the ellipse (the beam energy is more concentrated) to optimize the frequency offset.

In analytic geometry, the cross-term coefficient $b(f)$ represents the degree of inclination of the ellipse, and its value has nothing to do with the area. Without loss of generality, we set $b(f)$ to zero, (25) can be expressed as:

$$M^2 = a(f)\left(\frac{4\pi}{c}\right)^2 (r_h - r_t)^2 + G\left(\frac{2\pi f_0 d_T \cos\theta_t}{c}\right)^2 (\theta_h - \theta_t)^2. \tag{27}$$

Simplify (27) into an elliptical standard form.

$$\frac{(r_h - r_t)^2}{h_1^2} + \frac{(\theta_h - \theta_t)^2}{h_2^2} = 1,$$
$$h_1 = \frac{Mc}{\sqrt{a(f)}4\pi}, \tag{28}$$
$$h_2 = \frac{Mc}{\sqrt{G}2\pi f_0 d_T \cos\theta_t}.$$

The area of the ellipse can be expressed as:

$$S(\boldsymbol{f}) = \pi h_1 h_2 = \frac{M^2 c^2}{8\pi f_0 d_T \cos\theta_t} \frac{1}{\sqrt{a(\boldsymbol{f})G}}. \tag{29}$$

To facilitate the analysis, we rewrite the polynomial into a matrix form.

$$a(\boldsymbol{f})G = \boldsymbol{f}^T \boldsymbol{Q} \boldsymbol{f}, \tag{30}$$

$$\boldsymbol{Q} = \frac{M^3(M^2 - 1)}{3} \boldsymbol{I}_M - \frac{M^2(M^2 - 1)}{3} \boldsymbol{E}_M. \tag{31}$$

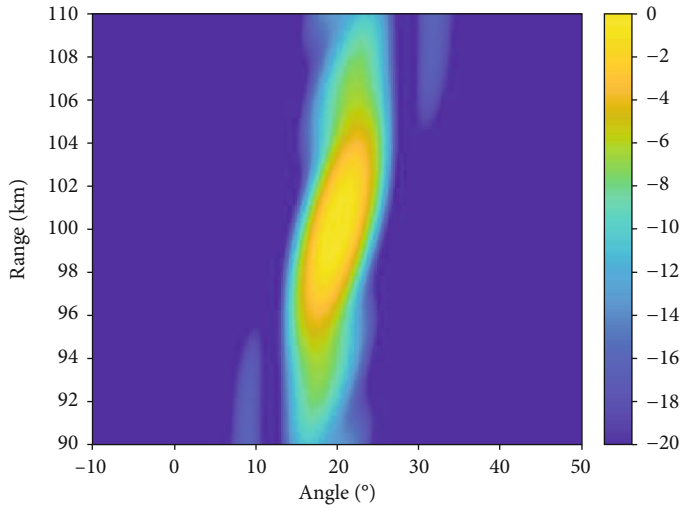

(a)

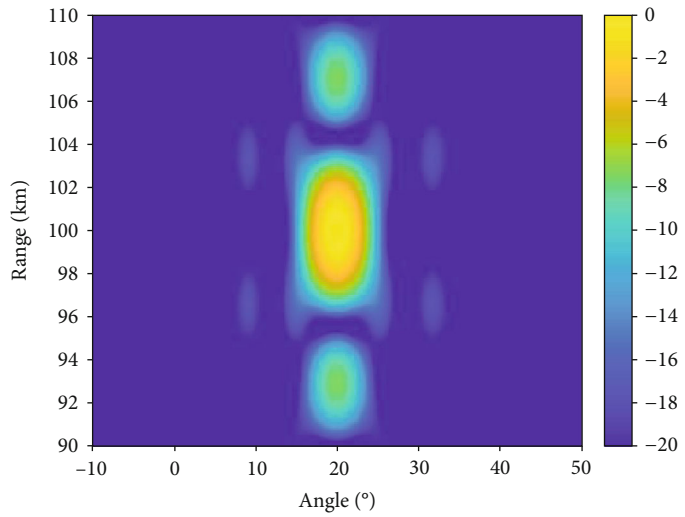

(b)

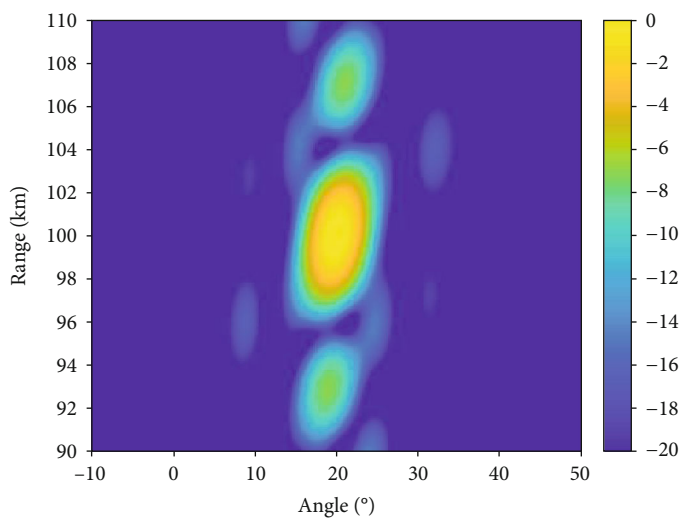

(c)

Figure 5: Continued.

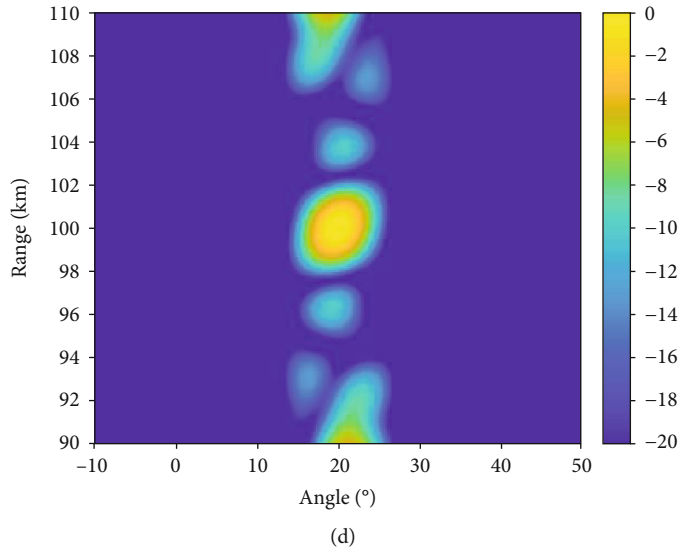

(d)

Figure 5: The equivalent transmit beampatterns at the receiver: (a) the beampattern of log_FDA; (b) the beampattern of Ham_FDA; (c) the beampattern of HL_FDA; (d) the beampattern of AM_FDA.

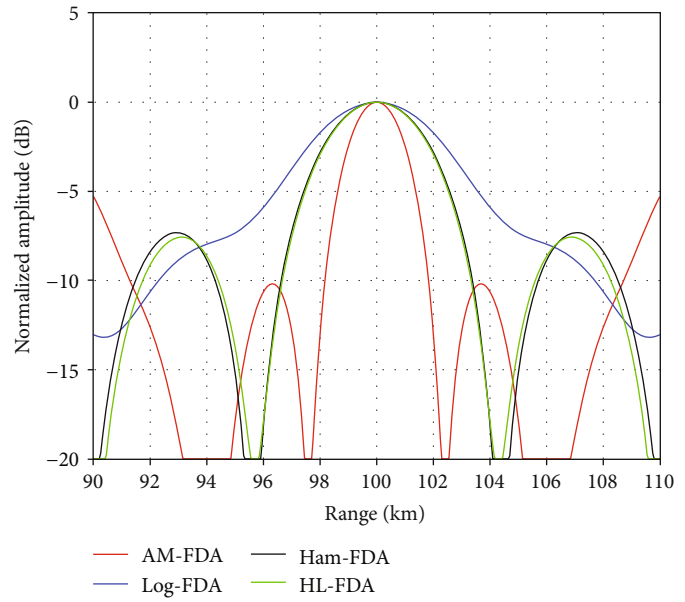

Figure 6: The equivalent transmit beampatterns in the profile of range.

The detailed derivation of (30) is provided by [22]. Bring (30) into (29), and rewrite (29) as:

$$S(\boldsymbol{f}) = \frac{M^2c^2}{8\pi f_0 d_T \cos\theta_t}\frac{1}{\sqrt{\boldsymbol{f}^T\boldsymbol{Q}\boldsymbol{f}}} \le \frac{M^2c^2}{8\pi f_0 d_T \cos\theta_t}\frac{1}{\sqrt{\lambda_{\boldsymbol{Q}\ \max}\boldsymbol{f}^T\boldsymbol{f}}}, \tag{32}$$

$$\lambda_{\boldsymbol{Q}\ \max}\boldsymbol{f}^T\boldsymbol{f} \ge \boldsymbol{f}^T\boldsymbol{Q}\boldsymbol{f}. \tag{33}$$

$\lambda_{\boldsymbol{Q}\ \max}$ is the maximum eigenvalue of matrix $\boldsymbol{Q}$, and only when $\boldsymbol{f} = \boldsymbol{f}_{\max}$ is the eigenvector corresponding to $\lambda_{\boldsymbol{Q}\ \max}$, the two sides of (33) are equal. Therefore, the smallest ellipse area is

$$S(\boldsymbol{f}) = \frac{M^2c^2}{8\pi f_0 d_T \cos\theta_t}\frac{1}{\sqrt{\lambda_{\boldsymbol{Q}\ \max}\boldsymbol{f}_{\max}{}^T\boldsymbol{f}_{\max}}}. \tag{34}$$

When the frequency offset of the transmitting array element is $\boldsymbol{f}_{\max}$, the area of the ellipse is the smallest. In other words, at this time, the main lobe area is the smallest, and the energy is more concentrated. In addition, $\boldsymbol{f}_{\max}$ is only related to matrix $\boldsymbol{Q}$, and matrix $\boldsymbol{Q}$is a real matrix that is only

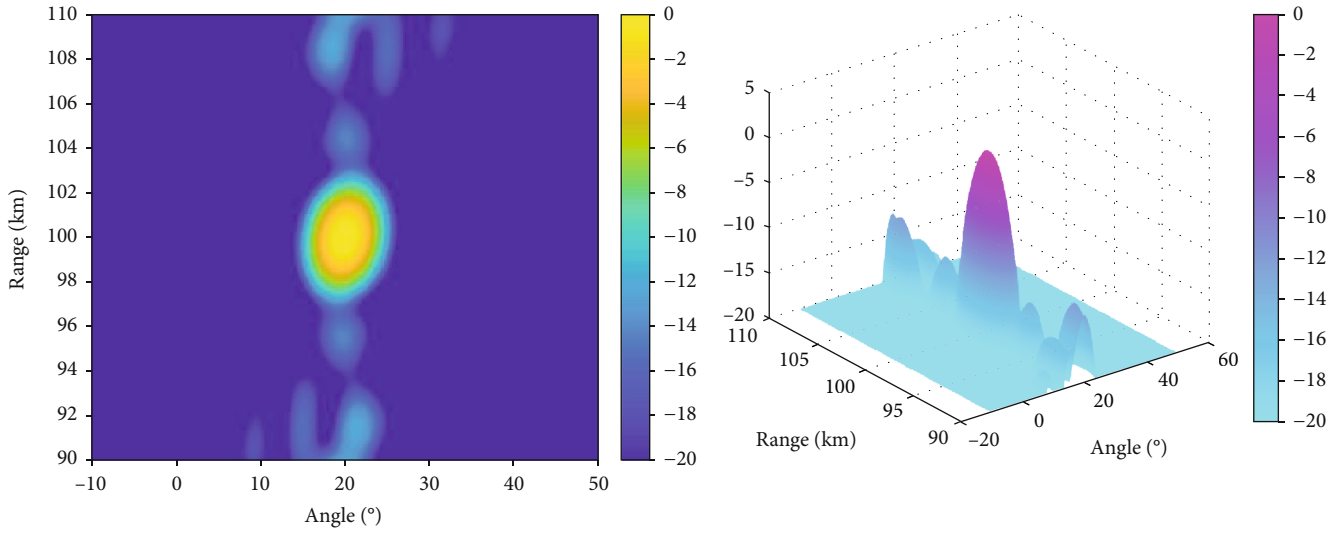

FIGURE 7: The equivalent transmit beampattern at the receiver: (a) the beampatterns of WAM_FDA (range-angle plane); (b) the beampatterns of WAM_FDA (3D).

related to the number of elements in the transmitting array. Therefore, $\boldsymbol{f}_{\max}$ is only related to the number of transmitting array elements. When the number of transmitting array elements is determined, we can determine the frequency offset required by each transmitting array element.

When the FDA-MIMO radar scans the space, we only need to change the parameters related to the target point (r_t, θ_t) in (12), and the frequency offset does not need to be reoptimized. Therefore, the method in this paper has lower time complexity than the method of using the optimization algorithm to solve the frequency offset.

5. Simulation Results

Many scholars have explored this to form a better beam. Logarithmically increasing frequency offset (Log_FDA) [14], Hamming window-based frequency offset (Ham_FDA) [16], and Hamming window weighted linear frequency increments (HL_FDA) [18] have been proposed. The proposed frequency offset scheme in our work is analytical method (AM_FDA). The frequency offset of the log-FDA can be expressed as:

$$\Delta f_m^{\log} = \delta_1 \log(m), \tag{35}$$

where δ_1 is a constant. Δf_m represents the frequency offset of the m-th transmitting array element. The frequency offset of the Ham_FDA is

$$\Delta f_m^{\text{Ham}} = B_w \left\{ 0.54 - 0.46 \cos\left(\frac{2\pi m}{2M_1}\right) \right\}, \tag{36}$$

where B_w is the bandwidth. M should satisfy:

$$M = 2M_1 + 1. \tag{37}$$

The frequency offset of the HL_FDA can be expressed as:

$$\Delta f_m^{\text{HL}} = (m-1)\delta_2 \left\{ 0.54 - 0.46 \cos\left(\frac{2\pi m}{2M_1}\right) \right\}, \tag{38}$$

where δ_2 is a constant. To obtain the frequency offset of the AM_FDA, we could use the function "eig" in the MATLAB. After many numerical experiments, the rank of matrix $\boldsymbol{Q}$ is always $M-1$, and there are $M-1$ eigenvectors corresponding to the largest eigenvalue $\lambda_{\boldsymbol{Q}\max}$. Hence, the frequency offset of the AM_FDA is

$$\begin{aligned} \boldsymbol{f} &= \delta_3 (k_1 \boldsymbol{f}_{\max 1} + k_2 \boldsymbol{f}_{\max 2} + \cdots + k_{M-1} \boldsymbol{f}_{\max M-1}), \\ &\in \text{span}(\boldsymbol{f}_{\max 1}, \boldsymbol{f}_{\max 2}, \cdots, \boldsymbol{f}_{\max M-1}), \end{aligned} \tag{39}$$

where δ_3 is a constant and $\boldsymbol{f} = [f(1), f(2), \cdots f(m) \cdots f(M)]$. $\text{span}(\boldsymbol{f}_{\max})$ represents the linear eigen subspace formed by $\boldsymbol{f}_{\max}$.

Without loss of generality, we set $k=1$. (39) rewrite as:

$$\boldsymbol{f} = \delta_3 (\boldsymbol{f}_{\max 1} + \boldsymbol{f}_{\max 2} + \cdots + \boldsymbol{f}_{\max M-1}). \tag{40}$$

The equivalent receiving beampattern is not affected by the frequency offset, and the frequency offset only affects the equivalent transmit beampattern. The equivalent receiving beampattern of each scheme is the same. Therefore, only the equivalent transmit beampattern is compared, in the simulation. We set the maximum frequency offset of the four methods to be similar to increase the credibility of the comparison, and the date below -20 dB is approximated to -20 dB in the beampattern measured in decibel to improve the comparing effects.

The carrier frequency is $f_0 = 10$Ghz, the number of elements is $M = N = 15$, transmitting element spacing and

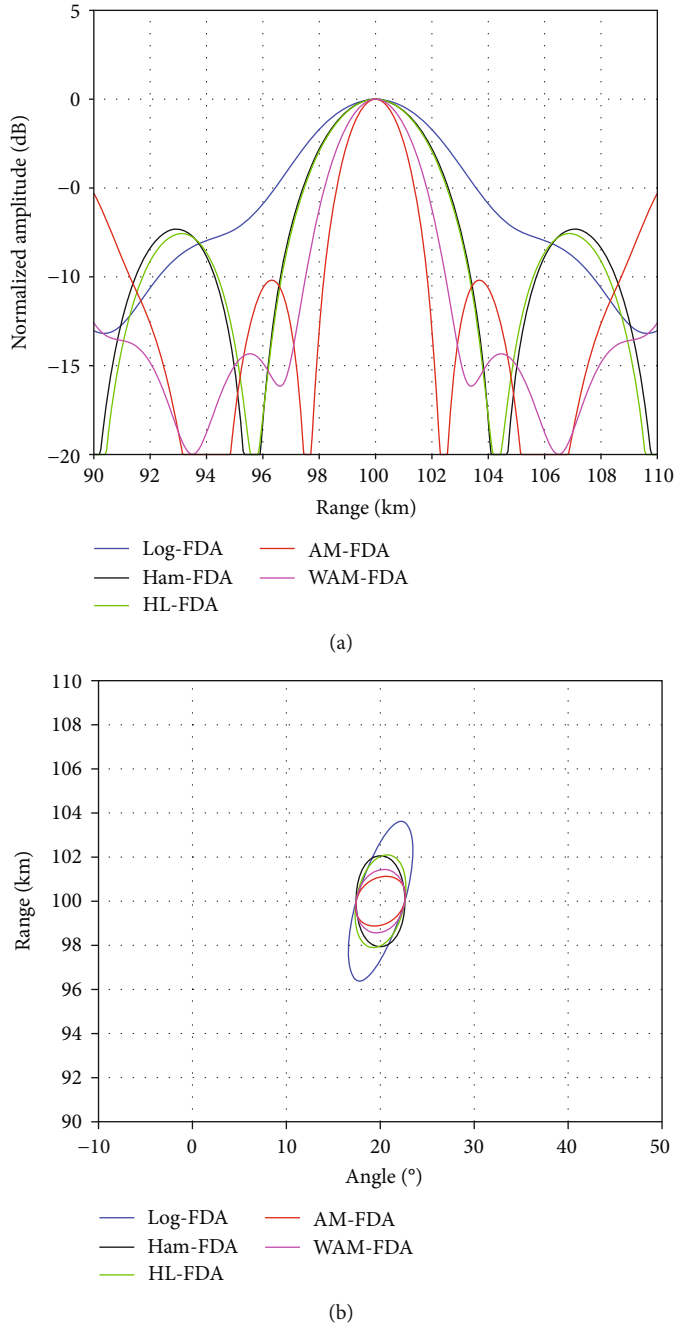

Figure 8: Comparative results of (a) the equivalent transmit beampatterns in the profile of range and (b) ellipses generated by different schemes.

receiving element spacing are both $d_T = d_R = 0.015m$, and the target is located at (100 km, 20°). The parameters related to frequency offset are set as follows: $\delta_1 = 10$kHz, $B_w = 27.5$ kHz, $\delta_2 = 3.5$kHz, and $\delta_3 = 18$kHz. The frequency offsets of log-FDA, Ham-FDA, HL_FDA, and our proposed AM_FDA are compared as shown in Figure 4. To eliminate unfairness, the maximum frequency offsets of these methods are approximately equal.

Based on using the time-invariant characteristics and range dependence of the FDA-MIMO radar system beampattern, we analyze the four schemes log_FDA, Ham_FDA, HL_FDA, and our proposed AM_FDA. The equivalent transmit beampattern of the four schemes at the receiver is shown in Figure 5.

It can be seen from Figure 5 that the shape of the main beam of each scheme is elliptical, which further verifies the correctness of formula (25). The beamwidth of log-FDA is the largest, and the beamwidth of AM_FDA is the smallest, which has better beam focusing and spatial resolution performance. When only range is considered, Ham-FDA, HL_FDA, and AM_FDA all form side lobes. The pattern performance is shown in Figure 6.

Figure 6 further shows that AM_FDA has a narrow beamwidth, forming a better beam. But AM _FDA also has a higher side lobe. As we all know, the reduction of the main lobe width will inevitably lead to an increase in the sidelobe level, because the total energy is constant. We use Kaiser window function weighting to reduce the sidelobe level (WAM_FDA), which will inevitably lead to an increase in the width of the main lobe. The frequency offset of the WAM_FDA is

$$\boldsymbol{f}_W = \boldsymbol{w}_M \boldsymbol{f}, \tag{41}$$

we could use the function "kaiser" in the MATLAB to obtain $\boldsymbol{w}_M$, where $\boldsymbol{w}_M = \text{kaiser}(M, \beta)$. We control the relationship between the main lobe and side lobes by adjusting β. The value of β can be determined according to the electromagnetic environment of the battlefield. Without loss of generality, we set $\beta = 2$.

Figures 7 and 8 show that when the side lobes decrease, the main lobe width increases, verifying the correctness of the theory. However, the HAM_FDA effectively reduces the side lobes, while the width of the main lobe increases less. Hence, the performance of HAM_FDA is better than other schemes.

In summary, using the FDA-MIMO radar system framework mentioned in this article can make full use of the range-related characteristics without being affected by time parameters. AM_FDA has good main lobe performance but has the disadvantage of the higher side lobe. WAM_FDA can better balance the relationship between the width of the main lobe and the level of the side lobe.

6. Conclusions

The design of frequency offset is a hot issue in FDA radar. In this paper, considering the influence of time parameters, taking the minimum main lobe as the optimized objective function, the optimal analytical solution of the frequency offset is obtained. Three aspects need to be emphasized. (1) The FDA-MIMO radar framework mentioned in this paper sets all frequency-related variables at the transmitter, and the frequency offset is only related to the number of transmit array elements, and finally, a range-dependent beampattern is obtained. (2) AM_FDA is significantly better than other solutions in range resolution. (3) Aiming at the problem of high sidelobe level, a window function method (WAM_FDA) is adopted to appropriately increase the width of the main lobe to reduce the sidelobe level.

Data Availability

The data used to support the findings of this study are available from the corresponding author upon request.

Conflicts of Interest

The authors declare that there are no conflicts of interest regarding the publication of this paper.

Acknowledgments

The author would like to thank Yezi Ma who gave enormous help to this work. This work was supported by the Aeronautical Science Foundation of China under grant 20190106002 and the China Postdoctoral Science Foundation under grant 2019M662257.

References

[1] P. Antonik, M. C. Wicks, H. D. Griffiths, and C. J. Baker, "Frequency diverse array radars," in *2006 IEEE Conference on Radar*, pp. 215–217, Verona, NY, Italy, April 2006.

[2] W. Wang, "Frequency diverse array antenna: new opportunities," *IEEE Antennas and Propagation Magazine*, vol. 57, no. 2, pp. 145–152, 2015.

[3] M. Secmen, S. Demir, A. Hizal, and T. Eker, "Frequency diverse array antenna with periodic time modulated pattern in range and angle," in *2007 IEEE Radar Conference*, pp. 427–430, Boston, MA, USA, April 2007.

[4] W.-Q. Wang, H. C. So, and A. Farina, "An overview on time/-frequency modulated array processing," *IEEE Journal of Selected Topics in Signal Processing*, vol. 11, no. 2, pp. 228–246, 2017.

[5] W. Wang, "Overview of frequency diverse array in radar and navigation applications," *IET Radar, Sonar & Navigation*, vol. 10, no. 6, pp. 1001–1012, 2016.

[6] H. C. So, M. G. Amin, S. Blunt, F. Gini, and W. Q. Wang, "Introduction to the special issue on time/frequency modulated array signal processing," *IEEE Journal of Selected Topics in Signal Processing*, vol. 11, no. 2, pp. 225–227, 2017.

[7] A.-M. Yao, W. Wu, and D.-G. Fang, "Solutions of time-invariant spatial focusing for multi-targets using time modulated frequency diverse antenna arrays," *IEEE Transactions on Antennas and Propagation*, vol. 65, no. 2, pp. 552–566, 2017.

[8] Q. Cheng, J. Zhu, T. Xie, J. Luo, and Z. Xu, "Time-invariant angle-range dependent directional modulation based on time-modulated frequency diverse arrays," *IEEE Access*, vol. 5, pp. 26279–26290, 2017.

[9] B. Chen, X. Chen, Y. Huang, and J. Guan, "Transmit beampattern synthesis for the FDA radar," *IEEE Antennas Wireless Propagation Letters*, vol. 17, no. 1, pp. 98–101, 2018.

[10] K. Chen, S. Yang, Y. Chen, and S. W. Qu, "Accurate models of time-invariant beampatterns for frequency diverse arrays," *IEEE Transactions on Antennas and Propagation*, vol. 67, no. 5, pp. 3022–3029, 2019.

[11] M. Tan, C. Wang, and Z. Li, "Correction analysis of frequency diverse array radar about time," *IEEE Transactions on Antennas and Propagation*, vol. 69, no. 2, pp. 834–847, 2021.

[12] J. Xu, J. Kang, G. Liao, and H. C. So, "Mainlobe deceptive jammer suppression with FDA-MIMO radar," in *2018 IEEE 10th Sensor Array and Multichannel Signal Processing Workshop (SAM)*, pp. 504–508, Sheffield, UK, July 2018.

[13] L. Lan, G. Liao, J. Xu, Y. Zhang, and F. Fioranelli, "Suppression approach to main-beam deceptive jamming in FDA-MIMO radar using nonhomogeneous sample detection," *IEEE Access*, vol. 6, pp. 34582–34597, 2018.

[14] W. Khan, I. M. Qureshi, and S. Saeed, "Frequency diverse array radar with logarithmically increasing frequency offset," *IEEE*

Antennas and Wireless Propagation Letters, vol. 14, pp. 499–502, 2015.

[15] Y. Wang, G. Huang, and W. Li, "Transmit beampattern design in range and angle domains for MIMO frequency diverse array radar," *IEEE Antennas and Propagation Letters*, vol. 16, no. 99, pp. 1003–1006, 2017.

[16] A. Basit, I. M. Qureshi, W. Khan, S. . Rehman, and M. M. Khan, "Beam pattern synthesis for an FDA radar with hamming window-based nonuniform frequency offset," *IEEE Antennas and Wireless Propagation Letters*, vol. 16, pp. 2283–2286, 2017.

[17] Y. Liao, H. Tang, X. Chen, and W.-Q. Wang, "Frequency diverse array beampattern synthesis with Taylor windowed frequency offsets," *IEEE Antennas and Wireless Propagation Letters*, vol. 14, no. 8, pp. 1–5, 2015.

[18] M. Tan, C. Wang, H. Yuan, J. Bai, and L. An, "FDA-MIMO beampattern synthesis with hamming window weighted linear frequency increments," *International Journal of Aerospace Engineering*, vol. 2020, 8 pages, 2020.

[19] J. Xiong, W. Wang, H. Shao, and H. Chen, "Frequency diverse array transmit beampattern optimization with genetic algorithm," *IEEE Antennas and Wireless Propagation Letters*, vol. 16, pp. 469–472, 2017.

[20] H. Shao, J. Dai, J. Xiong, H. Chen, and W. Q. Wang, "Dot-shaped range-angle beampattern synthesis for frequency diverse Array," *IEEE Antennas and Wireless Propagation Letters*, vol. 15, pp. 1703–1706, 2016.

[21] S. Y. Nusenu and A. Basit, "Frequency-modulated diverse array transmit beamforming with bat metaheuristic optimisation," *IET Radar, Sonar & Navigation*, vol. 14, no. 9, pp. 1338–1342, 2020.

[22] Y. Ma, P. Wei, and H. Zhang, "General focusing beamformer for FDA: mathematical model and resolution analysis," *IEEE Transactions on Antennas and Propagation*, vol. 67, no. 5, pp. 3089–3100, 2019.